IETE Journal of Research ›
Volume 69, 2023 - Issue 9

Articles

Quality of Life Modeling with Invulnerable Social-IoT Using Network Structural Entropy for Sustainable Smart City

Partha Sarathi Banerjee, Satyendra Nath Mandal, Debashis De & Biswajit Maiti

Pages 5813-5821 | Published online: 11 Jan 2023

Cite this article https://doi.org/10.1080/03772063.2022.2160840

Abstract

The Social Internet of Things (SIoT) builds up the communication architecture of state-of-the-art smart cities. Invulnerable IoT devices play a pivotal role in successfully deploying smart city services. The proposed model for Quality of Life (QoL) signifies the careful coordination between the smart APIs and the underlying devices, which are vulnerable to heavy traffic, security attacks and technical snags. Successful deployment of smart-city applications requires a proper quantification of the invulnerability of the IoT devices

against these adversaries. The empirical model, QoL, presents a technology-enabled quantitative measure to estimate the sustainability of the smart city with the help of device parameters.

KEYWORDS: Quality of life (QoL) Structural entropy Social IoT Sustainability Invulnerability Smart city

DISCLOSURE STATEMENT

No potential conflict of interest was reported by the author(s).

Additional information

Notes on contributors

Partha Sarathi Banerjee

Partha Sarathi Banerjee is currently working as an assistant professor of the Department of Information Technology of the Kalyani Government Engineering College,West-Bengal.

Satyendra Nath Mandal

Satyendra Nath Mandal He is currently working as an assistant professor in the Department of Information Technology of Kalyani Government Engineering College, West Bengal. **Email:** satyen_kgec@rediffmail.com

Debashis De

Debashis De is working as professor in the Department of Computer Science and Engineering of the Maulana Abul Kalam Azad University of Technology, West Bengal India. **Email:** dr.debashis.de@gmail.com

Biswajit Maiti

Biswajit Maiti is currently working as an associate professor in the Department of Physics at Maulana Azad College, Kolkata India. **Email:** bmkgec@gmail.com

Related Research

People also read | Recommended articles | Cited by

Application And Validity Analysis of IoT In Smart City Based On Entropy Method

Yejin Liu et al.
Applied Artificial Intelligence
Published online: 17 Jan 2023

Design of Internet of Things System Based Smart City Model on Raspberry Pi

Ajay Kumar et al.
IETE Journal of Research
Published online: 19 Jul 2022

CGARP: Chaos genetic algorithm-based relay node placement for multifaceted heterogeneous wireless sensor networks

S.I. : Multifaceted Intelligent Computing Systems (MICS) Published: 08 March 2022 (2022) Cite this article

Innovations in Systems and Software Engineering

Aims and scope

Submit manuscript

Partha Sarathi Banerjee, Satyendra Nath Mandal, Debashis De & Biswajit Maiti

Abstract

Relay node deployment in wireless sensor network (WSN) is significantly explored in specialized literature. There is a wide spectrum of performance issues like connectivity, coverage, energy efficiency, latency of packet delivery that have been considered as the target criteria to be optimized with the deployment strategies of relay nodes. The dynamic variation of different attributes of the sensor nodes leverages a heterogeneous topology. None of the literature has considered a heterogeneity-aware relay node placement strategy to pacify the effect of structural diversity on network performance. In this work, we propose chaos genetic algorithm-based relay node placement (CGARP) which takes care of the structural heterogeneity of WSN. CGARP is based on chaos genetic algorithm

(CGA), which overcomes the problem of premature convergence of genetic algorithm. *Tent Map*-based generation of the initial population and *Logistic Map*-based chaotic crossover enable CGARP to work well in WSN. The proposed technique has been compared with other relay node placement solutions available in the literature. CGARP achieves 68% improvement in average network lifetime in a 2D grid. It also results in 27% better connectivity and 23% improvement in the usage of relay nodes compared to EERP. The results are obtained through properly designed experiments with simulated realistic environments. These results substantiate the improvements achieved by the proposed approach.

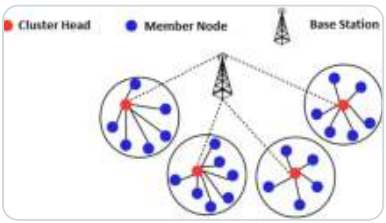

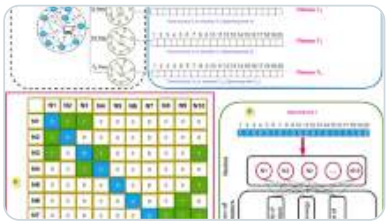

Availability of data and material

Data sharing is not applicable to this article as no datasets were generated or analyzed during the current study. All the data are generated based on the simulation of different parameters with theoretical constraints.

Code availability

The working environment for the current study has been designed in MATLAB by the authors. The codes are available with the corresponding author and can be shared with the respected Editors and Reviewers as and when required.

References

1. Akyildiz IF, Su W, Sankarasubramaniam Y, Cayirci E (2002) Wireless sensor networks: a survey. Comput Netw 38:393–422

Article Google Scholar

2. Vieira MAM, Coelho CN, Da Silva DC, da Mata JM (2003) Survey on wireless sensor network devices. In: Proceedings of IEEE Conference on Emerging Technology Fact. Autom., ETFA03, pp 537–544

3. Mohemed RE, Saleh AI, Abdelrazzak M, Samra AS (2017) Energy-efficient routing protocols for solving energy hole problem in wireless sensor networks. Comput Netw

114:51–66

Article Google Scholar

4. Chang J-H et al (2011) An efficient relay sensor placing algorithm for connectivity in wireless sensor networks. J Inf Sci Eng 27(1):381–392

MathSciNet Google Scholar

5. Djenouri D, Bagaa M (2017) Energy-aware constrained relay node deployment for sustainable wireless sensor networks. IEEE Trans Sustain Comput 2(1):30–42

Article Google Scholar

6. Ayinde BO, Barnawi AY (2014) Differential evolution based deployment of wireless sensor networks. In: 2014 IEEE/ACS 11th International Conference on Computer Systems and Applications (AICCSA). IEEE

7. Hashim HA, Bo A, Abido MA (2016) Optimal placement of relay nodes in wireless sensor network using artificial bee colony algorithm. J Netw Comput Appl 64:239–248

Article Google Scholar

8. Ayinde BO, Hashim HA (2018) Energy-efficient deployment of relay nodes in wireless sensor networks using evolutionary techniques. Int J Wireless Inf Networks 25(2):157–172

Article Google Scholar

9. Xu H, Huang L, Gang W, Zhang Y (2009) Spanner-aware relay node placement in wireless ad hoc sensor networks. In: Proceedings of the 5th International Conference on Mobile Ad-hoc and Sensor Networks (MSN), pp 180–186. https://doi.org/10.1109/MSN.2009.14.

10. Han B, Li J, Su J (2013) Optimal relay node placement for multi-pair cooperative communication in wireless networks. In: Proceedings of the IEEE Wireless Communications and Networking Conference (WCNC), pp 4724–4729. https://doi.org/10.1109/WCNC.2013.6555340 .

11. Misra S, Hong SD, Xue G, Tang J (2009) Constrained relay node placement in wireless sensor networks: formulation and approximations. IEEE/ACM Trans Netw 18(2):434–447

Article Google Scholar

12. Srivastava AK, Gupta SK (2019) EERP: energy-efficient relay node placement for *k*-connected wireless sensor networks using genetic algorithm. In: Hu YC, Tiwari S, Mishra K, Trivedi M (eds) Ambient communications and computer systems. Advances in intelligent systems and computing, vol 904. Springer, Singapore. https://doi.org/10.1007/978-981-13-5934-7_1

13. Azharuddin MD, Jana PK (2015) A GA-based approach for fault-tolerant relay node placement in wireless sensor networks. In: Proceedings of the 2015 Third International Conference on Computer, Communication, Control, and Information Technology (C3IT). IEEE, pp 1–6

14. Magán-Carrión R et al (2016) Optimal relay placement in multi-hop wireless networks. Ad Hoc Netw 46:23–36

Article Google Scholar

15. V. Mhatre, C. Rosenberg (2004) Homogeneous vs. heterogeneous clustered sensor networks: a comparative study. In: International Conference on Communication. IEEE, pp 3646–3651

16. Javidi M, Hosseinpourfard R (2015) Chaos Genetic Algorithm Instead Genetic Algorithm. Int Arab J Inf Technol (IAJIT) 12(2):1

17. Kim M, Leskovec J (2012) Multiplicative attribute graph model of real world networks. Internet Math 8(1–2):113–160

Article MathSciNet Google Scholar

18. Hu H-B, Wang X-F (2008) Unified index to quantifying heterogeneity of complex networks. Physica A 387(14):3769–3780

Article Google Scholar

19. Estrada E (2010) Quantifying network heterogeneity. Phys Rev E 82:066102

20. Rinku J, Harikrishnan KP, Mishra R, Ambika G et al (2017) Measure for degree hetero geneity in complex networks and its application to recurrence network analysis. R Soc Open Sci 4(1):1657

Google Scholar

21. Hu X, Leydesdorff L, Rousseau R (2017) Heterogeneity in an undirected network: definition and measurement. J Informet 11(2):669–682

Article Google Scholar

22. Li X, Zhou S, Lian G, Chen G, Liu J (2018) Heterogeneity of social network based on degree sequence and community. Int J Mod Phys B 32(30):1850331

Article MathSciNet Google Scholar

23. Hu H-B, Wang L (2005) The Gini coefficient's application to general complex networks. Adv Complex Syst 8(01):159–167

Article Google Scholar

24. Jun Wu, Yue-Jin T, Hong-Zhong D, Da-Zhi Z (2007) Normalized entropy of rank distribution: a novel measure of the heterogeneity of complex networks. Chin Phys 16(6):1576

Article Google Scholar

25. Wu J, Tan Y-J, Deng H-Z, Zhu D-Z (2007) Heterogeneity of scale-free networks. Syst Eng-Theory Pract 27(5):101–105

Article Google Scholar

26. Estrada E, Vargas-Estrada E (2012) Distance-sum heterogeneity in graphs and complex networks. Appl Math Comput 218(21):10393–10405

MathSciNet MATH Google Scholar

27. Safaei F, Tabrizchi S, Hadian Rasanan AH (2019) Zare M (2019) An energy-based heterogeneity measure for quantifying structural irregularity in complex networks. J Comput Sci 36:101011

Article MathSciNet Google Scholar

28. Ok C, Lee S, Mitra P, Kumara S (2010) Distributed routing in wireless sensor networks using energy welfare metric. Inf Sci 180(9):1656–1670

Article Google Scholar

29. Wei L, Sun W, Chen H, Yuan P, Yin F, Luo Q, Chen L (2018) A fast neighbor discovery algorithm in WSNs. Sensors 18(10):3319

Article Google Scholar

30. Sarathi BP, Mandal SN, De D, Maiti B (2022) MAHI: Multiple Attribute Heterogeneity Index for Wireless Sensor Networks. In: Proceedings of international conference on advanced computing applications. Springer, pp 299–312

31. Javidi M, Hosseinpourfard R (2015) Chaos Genetic Algorithm Instead Genetic Algorithm. Int Arab J Inf Technol (IAJIT) 12(2):1

Google Scholar

32. Snaselova P, Zboril F (2015) Genetic algorithm using a theory of chaos. Procedia Comput Sci 51:316–325

Article Google Scholar

33. Dai Lu, Wang B, Yang LT, Deng X, Yi L (2019) A nature-the inspired node deployment strategy for connected confident information coverage in dustrial Internet of Things. IEEE Internet Things J 6(6):9217–9225

Article Google Scholar

34. Chowdhury A, De D (2020) MSLG-RGSO: Movement score based limited grid-mobility approach using reverse Glowworm Swarm Optimization algorithm for mobile wireless sensor networks. Ad Hoc Networks 106:102191

35. Battiston F, Cencetti G, Iacopini I, Latora V, Lucas M, Patania A, Petri G (2020) Networks beyond pairwise interactions: structure and dynamics. Phys Rep

36. Gao X, Li K, Chen B (2017) Invulnerability measure of a military heterogeneous network based on network structure entropy. IEEE Access 6:6700–6708

Article Google Scholar

37. Yadav SL, Sohal A (2017) Study of the various selection techniques in genetic algorithms. Int J Eng Sci Math 6(3):198–204

38. Yadav SL, Sohal L (2017) Study of the various selection techniques in genetic algorithms. Int J Eng Sci Math 6(3):198–204

Acknowledgements

This work is an extended version of the paper entitled *"MAHI: Multiple Attribute Heterogeneity Index for Wireless Sensor Networks,"* accepted in the conference ICACA2021, AISC, Springer.

Funding

The authors did not receive any funds support from any organization for conducting the research mentioned in the submitted paper.

Author information

Authors and Affiliations

Kalyani Government Engineering College, Nadia, 741235, India
Partha Sarathi Banerjee & Satyendra Nath Mandal

Maulana Abul Kalam Azad University of Technology, West Bengal, Haringhata, West Bengal, India
Debashis De

Maulana Azad College, Kolkata, India
Biswajit Maiti

Contributions

P.S.B.: Conceptualization, Methodology, Simulation, Investigation, Formal Analysis, Writing-Original Draft. S.N.M.: Data curation, Methodology, Investigation, Reviewing and

Editing. D.D.: Conceptualization, Visualization, Supervision, Validation, Reviewing, and Editing. *B.M.:* Formal Analysis, Supervision, Reviewing and Editing.

Corresponding author

Correspondence to Partha Sarathi Banerjee.

Ethics declarations

Conflict of interest

All authors certify that they have no affiliations with or involvement in any organization or entity with any financial interest or non-financial interest in the subject matter or materials discussed in this manuscript.

Additional information

Publisher's Note

Springer Nature remains neutral with regard to jurisdictional claims in published maps and institutional affiliations.

Rights and permissions

Reprints and permissions

About this article

Cite this article

Banerjee, P.S., Mandal, S.N., De, D. *et al.* CGARP: Chaos genetic algorithm-based relay node placement for multifaceted heterogeneous wireless sensor networks. *Innovations Syst Softw Eng* (2022). https://doi.org/10.1007/s11334-022-00439-5

Received	Accepted	Published
30 May 2021	02 February 2022	08 March 2022

DOI

Calculation of Parameter of the Ashcroft Model Potential for Hexagonal Closed Pack (hcp) Crystals

A. Ghorai*

Department of Physics; Maulana Azad College 8, Rafi Ahmed Kidwai Road, Kolkata — 700013, India

(Received January 29, 2018; revised version July 4, 2018; in final form July 12, 2018)

Parameter of the Ashcroft model potential has been computed in this paper for twenty two hexagonal closed pack (hcp) crystals. Calculation uses pseudopotential technique with nine different exchange and correlation functions and either available experimental value of monovacancy formation energy or an empirical relation based on other experimental parameters (melting temperature, cohesive energy or activation energy) as tool. The complete set of value of this parameter for cubic crystals will be used for further calculation of energetic of self and impurity diffusion via vacancy mechanism or other type of point defects.

DOI: 10.12693/APhysPolA.134.549

PACS/topics: point defect, vacancy, pseudopotential, Ashcroft model, hcp crystal

1. Introduction

The pseudopotential approach has been tested earlier several times [1–3] and in this paper this formalism is applied to twenty two different hexagonal closed pack (hcp) crystals, viz. (1) beryllium (Be), (2) magnesium (Mg), (3) scandium (Sc), (4) titanium (Ti), (5) cobalt (Co), (6) zinc (Zn), (7) yttrium (Y), (8) zirconium (Zr), (9) technetium (Tc), (10) ruthenium (Ru), (11) cadmium (Cd), (12) gadolinium (Gd), (13) terbium (Tb), (14) dysprosium (Dy),(15) holmium (Ho), (16) erbium (Er), (17) thullium (Tm), (18) lutetium (Lu), (19) hafnium (Hf), (20) rhenium (Re), (21) osmium (Os) and (22) thallium (Tl) (arranged according to increasing atomic number). Although *ab initio*, DFT, molecular dynamics, etc. calculations are most sophisticated techniques yet they lack exact predictions when applied to defect property calculations. In this situation this work is important because rigorous computation is not required as in above new methodologies. Secondly it is comparatively easier technique and thirdly there are very few data of point defect parameters for hcp crystals. Especially out of 22 hcp crystals experimental evidence of monovacancy formation energy is obtained for only six. So an empirical relation among cohesive energy, melting temperature, activation energy for self diffusion, and monovacancy formation energy is used for theoretical estimation. Also it is important because of recent studies of the mechanism of melting [4, 5] by considering the role of surfaces with regard to the concentration and migration of vacancies. Lattice instability occurs both at the surface and within the crystal lattice when the vacancy concentration increases from 0.37% to 10% on melting.

2. Formulations

Harrison's second order perturbation theory gives the total energy of the pure crystal as [3]:

$$E_T = z\left[\frac{3\hbar^2 k_{\mathrm{F}}^2}{10m} + \langle \boldsymbol{k}|W(r)|\boldsymbol{k}\rangle\right] + E_{bs} + E_{es}. \tag{1}$$

Here z is the valency, k_{F} — the Fermi wave number, m — the electronic mass, and $W(r)$ — the pseudopotential. The first term within square bracket is structure independent and the last two terms, called the electrostatic energy E_{es} (depends on ion–ion interaction) and the band structure energy E_{bs} (depends on ion–electron and electron–electron interactions) depend on the crystal structure. Any defect in the lattice changes the structure dependent energy part of E_T and so an algebraic difference between the energy after defect creation and that before will yield the defect formation energy when considered for the whole lattice. This structure dependent part of E_T also depends on the modified lattice wave numbers. The modifications in the lattice wave numbers from its perfect lattice value, is necessary to maintain the lattice volume and the number of lattice ions constant. Details of it can be obtained from literature and finally the expression for vacancy formation energy is

$$E_{\mathrm{F}}^{1v} = \sum\nolimits_{q_0}{}' \frac{q_0}{3}\frac{\partial U(q_0)}{\partial q_0} + \frac{\Omega}{2\pi^2}\int_0^{\infty} U(q)\, q^2\, \mathrm{d}q, \tag{2}$$

where

$$U(q) = \lim_{\eta\to\infty} \frac{2\pi z^2 e^2}{\Omega q^2}\, \mathrm{e}^{-\frac{q^2}{4\eta}} + [\omega(q)]^2 \varepsilon(q)\chi(q) \tag{3}$$

Here η is the convergence factor, Ω — the atomic volume, $\boldsymbol{q}_0$ and $\boldsymbol{q}$ — the lattice and quasi-continuous wave numbers respectively, $\omega(q)$ — the pseudopotential, $\varepsilon(q)$ — the dielectric function, and $\chi(q)$ — the perturbation characteristics. Here I have considered the Ashcroft model pseudopotential [6], which is

$$w(q) = -\frac{4\pi z e^2 \cos q r_c}{\Omega q^2}. \tag{4}$$

Here r_c is the parameter for the Ashcroft model. The expressions for $\varepsilon(q)$ and $\chi(q)$ are

$$\varepsilon(q) = 1 - \frac{8\pi \mathrm{e}^2}{\Omega q^2}[1 - f(q)]\chi(q) \tag{5}$$

*e-mail: amitavaghorai@rediffmail.com

$$\chi(q) = -\frac{mk_{\mathrm{F}}\Omega}{4\pi^2\hbar^2}\left(1 + \frac{4k_{\mathrm{F}}^2 - q^2}{4k_{\mathrm{F}}q}\ln\frac{|2k_{\mathrm{F}} + q|}{|2k_{\mathrm{F}} - q|}\right) \tag{6}$$

Here $f(q)$ is the exchange and correlation function (hence forth called ECF). Out of several ECFs only nine such forms are taken into account and the expressions [1] are

King and Kutler ECF (abbreviated henceforth as K-K)

$$f(q) = \frac{q^2}{2(2k_{\mathrm{F}}^2 + q^2)}, \tag{7}$$

Sham ECF (abbreviated as Sham)

$$f(q) = \frac{q^2}{2(k_{\mathrm{F}}^2 + q^2 + \frac{2k_{\mathrm{F}}}{\pi a_0})}, \tag{8}$$

Geldart and Vosko ECF (abbreviated as G-V)

$$f(q) = \frac{q^2}{2q^2 + 4k_{\mathrm{F}}^2/\left(1 + \frac{0.026m'}{m}\sqrt[3]{\frac{3\Omega}{4\pi z a_0^3}}\right)}, \tag{9}$$

Kleinmann ECF (abbreviated as Kle)

$$f(q) = \frac{1}{4}\left(\frac{q^2}{k_{\mathrm{F}}^2 + \frac{2k_{\mathrm{F}}}{\pi a_0}} + \frac{q^2}{k_{\mathrm{F}}^2 + q^2 + \frac{2k_{\mathrm{F}}}{\pi a_0}}\right), \tag{10}$$

Harrison ECF (abbreviated as Harr)

$$f(q) = \frac{q^2}{2\left(q^2 + \frac{4k_{\mathrm{F}}^2}{3}\right)}, \tag{11}$$

Vashishta and Singwi ECF (abbreviated as V-S)

$$f(q) = A\left(1 - \mathrm{e}^{-\frac{Bq^2}{k_{\mathrm{F}}^2}}\right), \tag{12}$$

Taylor ECF (abbreviated as Tay)

$$f(q) = \frac{q^2}{4k_{\mathrm{F}}^2}\left(1 + \frac{0.1534}{\pi k_{\mathrm{F}}}\right), \tag{13}$$

Hubbard ECF (abbreviated as Hub)

$$f(q) = \frac{q^2}{2(k_{\mathrm{F}}^2 + q^2)}, \tag{14}$$

Mahanti and Das ECF (abbreviated as M-D)

$$f(q) = \frac{q^2}{k_{\mathrm{F}}^2 + 4k_{\mathrm{F}}^2/\left(1 + \frac{0.026m'}{m}\sqrt[3]{\frac{3\Omega}{4\pi z a_0^3}}\right)} + \frac{q^2}{k_{\mathrm{F}}^2 + q^2 + 4k_{\mathrm{F}}^2/\left(1 + \frac{0.026m'}{m}\sqrt[3]{\frac{3\Omega}{4\pi z a_0^3}}\right)}. \tag{15}$$

Here a_0 is the Bohr radius. Computation has been done by integration over quasi-continuous wave numbers $\boldsymbol{q}$ using the Gauss–Legendre quadrature integration within the limit from 0 to 1 in 100 divisions and Gauss–Laguerre quadrature integration in the limit from 1 to infinity as follows:

$$\int_0^\infty \rightarrow \int_0^1 \text{Gauss-Legendre} + \int_1^\infty \text{Gauss-Laguerre}. \tag{16}$$

Computation also uses a discrete sum over lattice wave numbers $\boldsymbol{q}_0$ with primitive and reciprocal lattice vectors are defined respectively as

$$\boldsymbol{a}_1 = \frac{\sqrt{3}a}{2}\widehat{i} + \frac{a}{2}\widehat{j}, \quad \boldsymbol{a}_2 = -\frac{\sqrt{3}a}{2}\widehat{i} + \frac{a}{2}\widehat{j},$$
$$\boldsymbol{a}_3 = c\widehat{k} \tag{17}$$

$$\boldsymbol{q}_1 = \frac{2\pi}{\sqrt{3}a}(\widehat{i} + \sqrt{3}\widehat{j}), \quad \boldsymbol{q}_2 = \frac{2\pi}{\sqrt{3}a}(-\widehat{i} + \sqrt{3}\widehat{j}),$$
$$\boldsymbol{q}_3 = \frac{2\pi}{c}\widehat{k} \tag{18}$$

with

$$\boldsymbol{q}_0 = \frac{m_1}{N_1}\boldsymbol{q}_1 + \frac{m_2}{N_2}\boldsymbol{q}_2 + \frac{m_3}{N_3}\boldsymbol{q}_3. \tag{19}$$

The maximum value of $m_i/N_i = 14$ with $i = 1, 2, 3$ and the lattice wave numbers are generated in the cubic Brillouin zone. Here a and c are lattice constants of hcp crystal.

3. Discussions

The input parameters used in this calculation are lattice constant (a and c) and experimental value of vacancy formation energy $(E_{\mathrm{F}}^{1v})_{\mathrm{exp}}$ or theoretical mean value of it $(E_{\mathrm{F}}^{1v})_{\mathrm{fit}}$. The necessity of $(E_{\mathrm{F}}^{1v})_{\mathrm{fit}}$ is due to the fact that in most of the cases the experimental value of E_{F}^{1v} is not available and so $(E_{\mathrm{F}}^{1v})_{fit}$ is determined from an empirical relation among the melting temperature (T_m), the cohesive energy (E_{coh}), the activation energy (Q_0) and monovacancy formation energy (E_{F}^{1v}) as

$$T_m(\mathrm{K}) = 1200E_{\mathrm{F}}^{1v}(\mathrm{eV}) = 660Q_0(\mathrm{eV}) = 360E_{\mathrm{coh}}(\mathrm{eV}). \tag{20}$$

Earlier several researchers used different experimental results, viz. resistivity, phonon dispersion relation, etc. to determine parameter of the Ashcroft model potential r_c and here experimental or mean theoretical estimation of E_{F}^{1v} is used to determine r_c. Comparison is done with available other theoretical values of E_{F}^{1v} which are shown in Table I. Our fitted value of $(E_{\mathrm{F}}^{1v})_{\mathrm{fit}}$ is very close to the Angsten et al. estimated values [8].

The variation of E_{F}^{1v} in rydbergs (1 Ry= 13.605 eV) with the Ashcroft parameter r_c are shown in Figs. 1–4 within zero to 5 AU (1 AU = 0.0529177 nm). The graphs are almost similar for all exchange and correlation functions because of square of cosine term of the Ashcroft model. The available experimental value of E_{F}^{1v} is found to lie near the first nodal point corresponding to the condition $E_{\mathrm{F}}^{1v} \rightarrow 0$ and $a_0 \leq r_c < 2AU$ where $a_0(= 1\ \mathrm{AU})$ is the Bohr radius. The fitted value of r_c is shown in Table II for different ECFs.

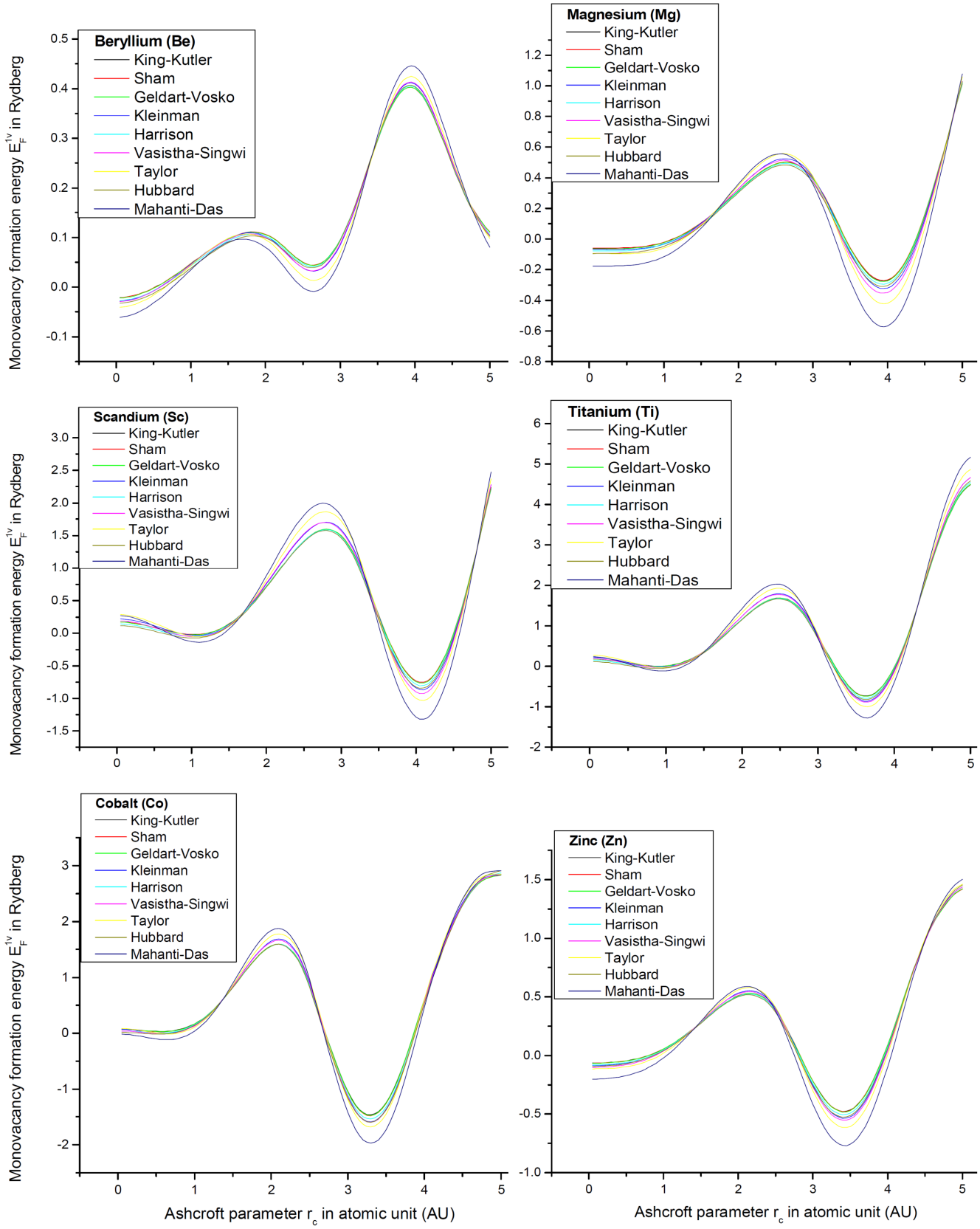

Fig. 1. $E_F^{1v} - r_c$ plots for for beryllium (Be), magnesium (Mg), scandium (Sc), titanium (Ti), cobalt (Co), zinc (Zn).

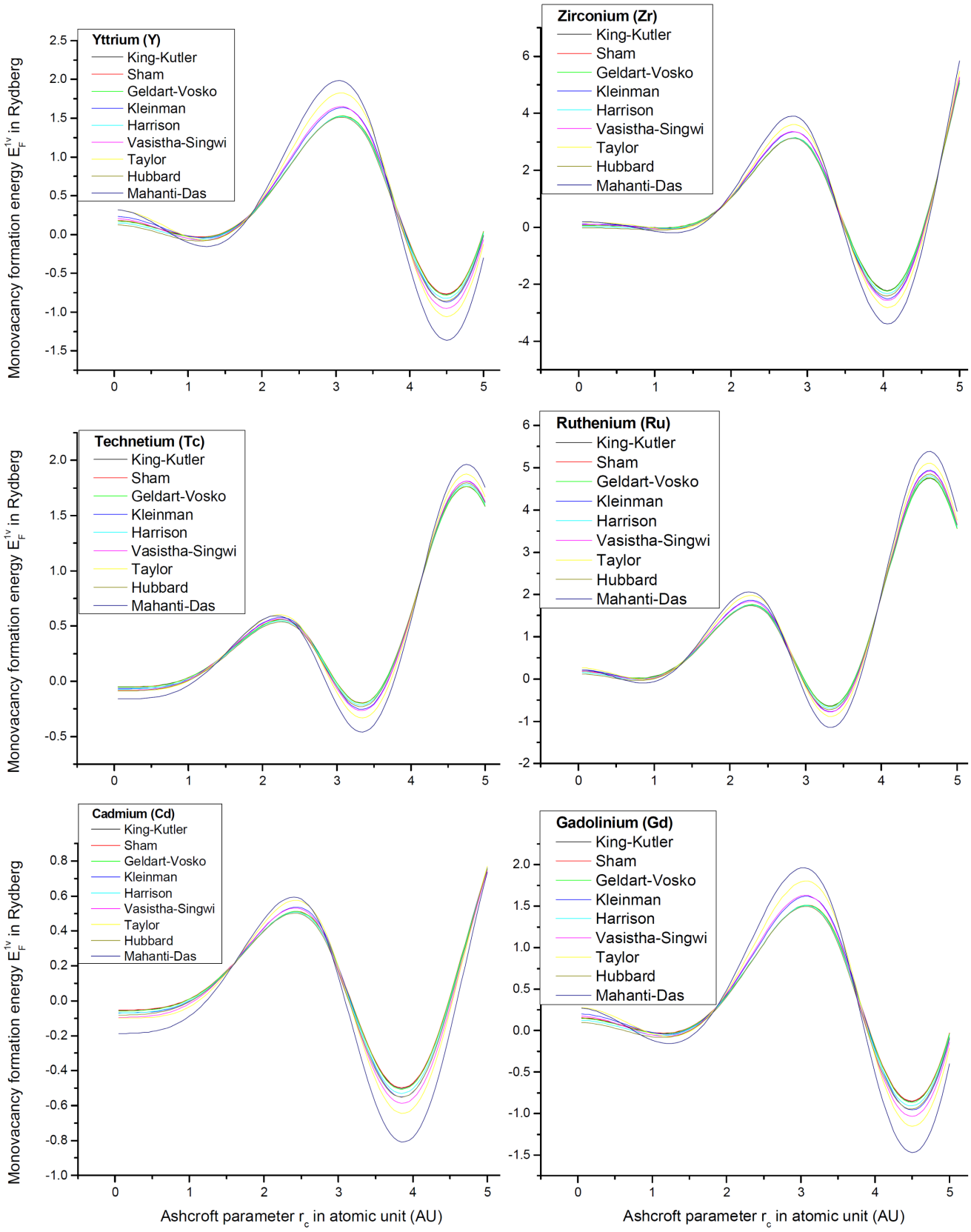

Fig. 2. $E_F^{1v} - r_c$ plots for yttrium (Y), zirconium (Zr), technetium (Tc), ruthenium (Ru), cadmium (Cd), gadolinium (Gd).

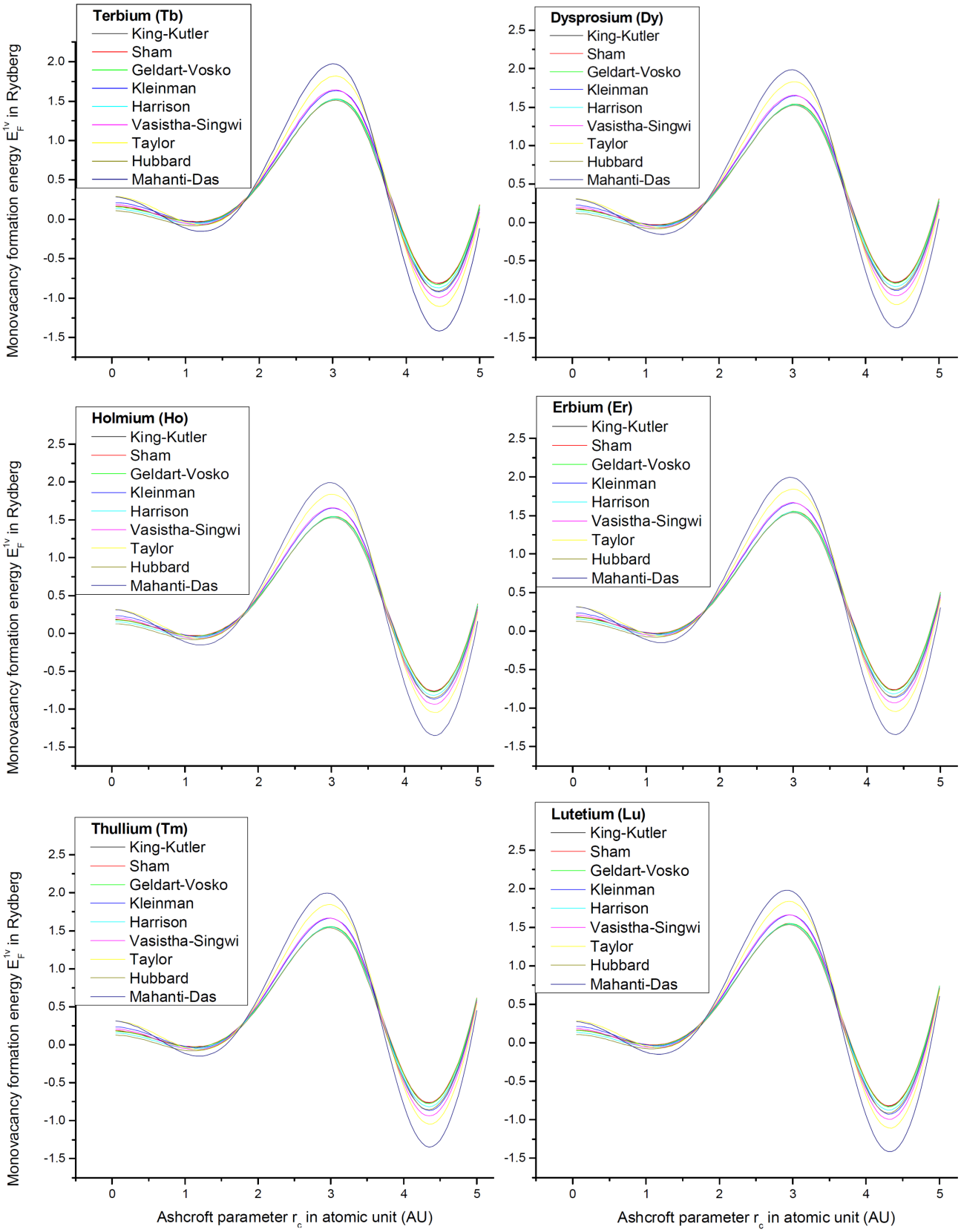

Fig. 3. $E_{\mathrm{F}}^{1v} - r_c$ plots for terbium (Tb), dysprosium (Dy), holmium (Ho), erbium (Er), thulium (Tm), lutetium (Lu).

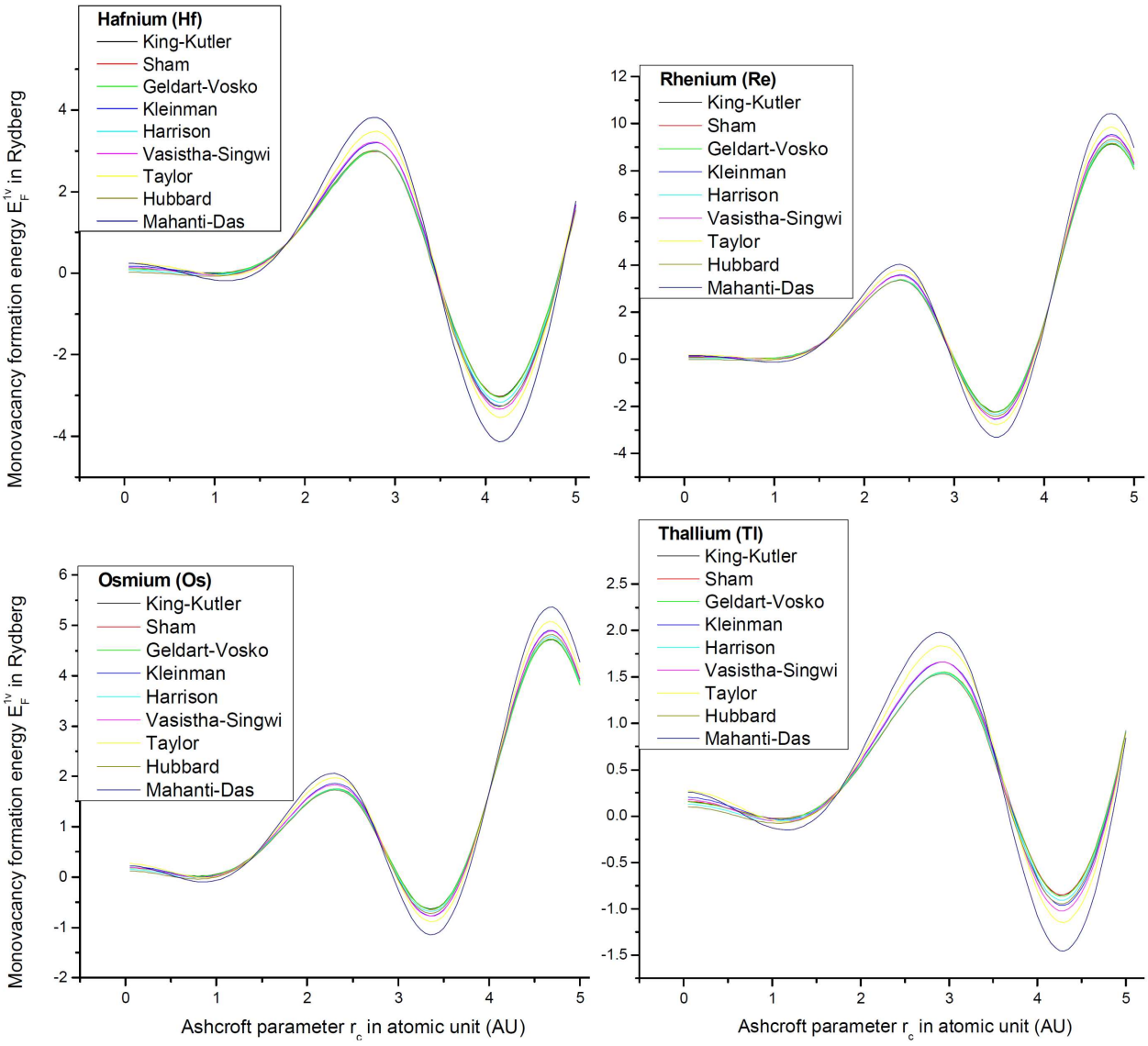

Fig. 4. $E_{\mathrm{F}}^{1v} - r_c$ plots for hafnium (Hf), rhenium (Re) IV, osmium (Os) III, thallium (Tl) III.

The correct value of valency in crystalline state has been chosen out of multiple values by noting that the Ashcroft parameter r_c lies near to first peak and the Bohr radius. A graph shown in Fig. 5 for atomic number and fitted r_c for different fcc [1] and hcp cubic crystals satisfies this idea. Thus out of two valence states (1, 2) for beryllium $z = 1$ has been chosen. Similarly for other multi-valent metals like titanium, cobalt, technetium, ruthenium, terbium, rhenium, osmium and thallium the valency values corresponding to lowest r_c values are listed in Table I.

The variation of the Ashcroft parameter r_c with different exchange and correlation functions for different hcp crystals is shown in Table II with the mean value. The value of r_c in cases of cobalt and zinc show slightly less than the Bohr radius. This may be due to less estimation of $(E_{\mathrm{F}}^{1v})_{fit}$ because of higher calculated values

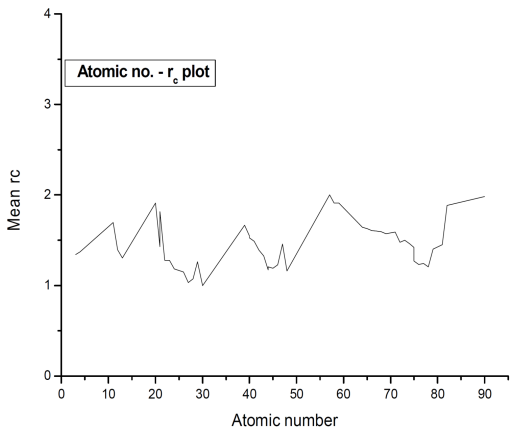

Fig. 5. Mean Ashcroft parameter r_c for hcp and fcc crystals.

TABLE I

Input parameters for hexagonal closed pack (hcp) crystals

Element	Atomic no.	z	a^a [nm]	c^a [nm]	V-S parameters		T_m^a	$E_{\rm coh}^a$	Q_0^b	$(E_{\rm F}^{1v})_{\rm fit}$	$(E_{\rm F}^{1v})_{\rm Th}^b$	$(E_{\rm F}^{1v})_{\rm exp}$
					A in AU	B in AU	[K]	[eV]	[eV]	[eV]	[eV]	[eV]
Beryllium (Be)	4	1	0.227	0.359	0.8079	0.3435	1562	3.32		1.149	1.04	
Magnesium (Mg)	12	2	0.321	0.521	0.9009	0.3211	922	1.51	1.30	0.645	0.78	$0.80^{f,g}$
Scandium (Sc)	21	3	0.331	0.521	0.9096	0.3257	1814	3.9		1.341	1.87	0.96^{c}
Titanium (Ti)	22	3	0.295	0.468	0.8769	0.3264	1946	4.85	3.14	1.601	2.06	
Cobalt (Co)	27	3	0.251	0.407	0.8338	0.3368	1770	4.39		1.396	1.67, 1.93	
Zinc (Zn)	30	2	0.266	0.495	0.8496	0.3326	692.7	1.35	1	0.511	0.47	$0.54^{c,g}$
Yttrium (Y)	39	3	0.365	0.573	0.9409	0.3193	1801	4.37		1.406	1.87	
Zirconium (Zr)	40	4	0.323	0.515	0.9026	0.3264	2128	6.25	3.17	1.797	2.03	
Technetium (Tc)	43	2	0.274	0.44	0.8579	0.3305	2477	6.85		2.060	0.25	
Ruthenium (Ru)	44	3	0.271	0.428	0.8554	0.3311	2527	6.74		2.064	2.68	
Cadmium (Cd)	48	2	0.298	0.562	0.8799	0.3326	594.3	1.16	0.86	0.439	0.25	0.46^{d}
Gadolinium (Gd)	64	3	0.363	0.578	0.9390	0.3122	1587	4.14		1.282		
Terbium (Tb)	65	3	0.36	0.57	0.9360	0.3130	1632	4.05		1.288		
Dysprosium (Dy)	66	3	0.359	0.565	0.9352	0.3137	1684	3.04		1.158		
Holmium (Ho)	67	3	0.358	0.562	0.9343	0.3139	1745	3.14		1.198		
Erbium (Er)	68	3	0.356	0.559	0.9324	0.3138	1797	3.29		1.242		
Thulium (Tm)	69	3	0.354	0.556	0.9306	0.3147	1820	2.42		1.121		
Lutetium (Lu)	71	3	0.35	0.555	0.9270	0.3155	1938	4.43		1.472		
Hafnium (Hf)	72	4	0.319	0.505	0.8991	0.3214	2504	6.44	3.35	1.954	2.26	2.45^{e}
Rhenium (Re)	75	4	0.276	0.446	0.8597	0.3302	3459	8.03		2.646	3.42	
Osmium (Os)	76	3	0.274	0.432	0.8579	0.3306	3306	8.17		2.603	3.03	
Thallium (Tl)	81	3	0.346	0.552	0.9234	0.3103	577	1.88	1.04	0.539	0.40	$0.46^{d,f}$

[a] Ref. [7]; [b] Ref. [8]; [c] Ref. [9]; [d] Ref. [10]; [e] Ref. [11]; [f] Ref. [12]; [g] Ref. [13]

TABLE II

Variation of the Ashcroft parameter with ECFs for different hcp crystals.

hcp crystal	r_c in AU fitted to $(E_{\rm F}^{1v})_{\rm exp}$ or $(E_{\rm F}^{1v})_{\rm fit}$									
	K-K	Sham	G-V	Kle	Harr	V-S	Tay	Hub	M-D	Mean
Beryllium (Be)	1.3466	1.3473	1.3538	1.3427	1.3930	1.3585	1.3408	1.4384	1.4154	1.3707
Magnesium (Mg)	1.3590	1.3551	1.3648	1.3792	1.3912	1.3975	1.4208	1.4188	1.4751	1.3957
Scandium (Sc)	1.3849	1.3853	1.3916	1.4136	1.4210	1.4320	1.4501	1.4505	1.5054	1.4260
Titanium (Ti)	1.2429	1.2506	1.2512	1.2727	1.2758	1.2790	1.2954	1.3005	1.3420	1.2789
Cobalt (Co)	0.8856	0.9025	0.8979	0.9534	0.9244	0.9595	0.9916	0.9447	1.0618	0.9468
Zinc (Zn)	0.9432	0.9447	0.9512	0.9946	0.9737	1.0067	1.0487	0.9951	1.1168	0.9972
Yttrium (Y)	1.6359	1.6328	1.6409	1.6528	1.6633	1.6694	1.6822	1.6864	1.7224	1.6651
Zirconium (Zr)	1.4970	1.5017	1.5022	1.5468	1.5278	1.5483	1.5902	1.5530	1.6622	1.5477
Technetium (Tc)	1.3090	1.3103	1.3122	1.3168	1.3305	1.3199	1.3254	1.3507	1.3529	1.3253
Ruthenium (Ru)	1.1420	1.1517	1.1485	1.1706	1.1722	1.1717	1.1853	1.1954	1.2279	1.1739
Cadmium (Cd)	1.1015	1.0985	1.1069	1.1488	1.1290	1.1757	1.2200	1.1506	1.2960	1.1586
Gadolinium (Gd)	1.6128	1.6103	1.6184	1.6311	1.6389	1.6506	1.6686	1.6655	1.7129	1.6455
Terbium (Tb)	1.5955	1.5930	1.6015	1.6150	1.6241	1.6313	1.6497	1.6485	1.6930	1.6279
Dysprosium (Dy)	1.5714	1.5685	1.5769	1.5920	1.6027	1.6101	1.6269	1.6272	1.6737	1.6055
Holmium (Ho)	1.5697	1.5675	1.5750	1.5899	1.6007	1.6070	1.6228	1.6250	1.6684	1.6029
Erbium (Er)	1.5637	1.5614	1.5689	1.5829	1.5937	1.6001	1.6156	1.6179	1.6605	1.5961
Thulium(Tm)	1.5317	1.5300	1.5383	1.5587	1.5684	1.5761	1.5934	1.5944	1.6415	1.5703
Lutetium (Lu)	1.5589	1.5573	1.5635	1.5774	1.5862	1.5916	1.6077	1.6088	1.6491	1.5889
Hafnium (Hf)	1.4356	1.4381	1.4393	1.4801	1.4583	1.4874	1.5242	1.4733	1.5715	1.4786
Rhenium (Re)	1.2260	1.2368	1.2306	1.2757	1.2587	1.2691	1.3046	1.2830	1.3508	1.2706
Osmium (Os)	1.2088	1.2135	1.2118	1.2273	1.2300	1.2275	1.2353	1.2516	1.2736	1.2310
Thallium (Tl)	1.3945	1.3925	1.4033	1.4316	1.4409	1.4574	1.4862	1.4749	1.5578	1.4488

of $(E_{\mathrm{F}}^{1v})_{Th}$ for cobalt by Angsten et al. [8]. However for zinc the experimental value of $(E_{\mathrm{F}}^{1v})_{\mathrm{exp}}$ is higher than all the theoretical estimates and average value of r_c is very close to one AU.

I started computing defect energy calculation using simple model of Ashcroft which contains only one parameter. The complete set of value of r_c for cubic crystals will be used for further calculation of energetic of self and impurity diffusion via vacancy mechanism or other type of point defects. The work with two-parameter Heine–Abarenkov model is under progress.

References

[1] A. Ghorai, *Def. Diff. Forum* **329**, 81 (2012).

[2] A. Ghorai, *Phys. Rev. B* **46**, 5229 (1992).

[3] W.A. Harrison, *Pseudopotentials in the Theory of Metals*, Benjamin, New York 1966.

[4] Q.S. Mei, K. Lu, *Philos. Mag. Lett.* **88**, 203 (2008).

[5] Lianwen Wang, *Metals* **2014**, 570 (2014).

[6] N.W. Ashcroft, *Phys. Lett.* **23**, 48 (1966).

[7] C. Kittel, *Introduction to Solid State Physics*, 5th ed., Wiley Eastern, New Delhi 1979.

[8] T. Angsten, T. Mayeshiba, H. Wu, D. Morgan, *New J. Phys.* **16**, 015018 (2014).

[9] S. Chattopadhyay, A. Ghorai, in: *Proc. CMDays 2014, held at Dept. of Phys., University of Calcutta*, 2014.

[10] D. Bhattacharya, A. Ghorai, in: *Proc. CMDays 2014, held at Dept. of Phys., University of Calcutta*, 2014.

[11] G. Vérité, F. Willaime, Chu Chun Fu, *Solid State Phenom.* **129**, 75 (2007).

[12] P. Tzanetakis, J. Hillairet, G. Revel, *Phys. Status Solidi B* **75**, 433 (1976).

[13] E.V. Chulkov, *Sov. Phys. J.* **25**, 191 (1982).

Some Workout Problems on Motion of Raindrop

Sneha Dey[1,2] and A. Ghorai[2]

[1]Physics Department, Maulana Azad College
Kolkata, India
Email: sneha072000 [AT] gmail.com

[2]School of Science, Jangalpur Road
Kolkata, India
Email: amitavaghorai61 [AT] gmail.com

ABSTRACT— ***The motion of rain drop through atmosphere is an interesting classical problem because of the fact that air resistance and moisture accretion are integral part of it. Mathematical modeling of it using Newtonian formalism is considered here and discussions are made for no mass accretion and air resistance proportional to nth power of velocity. We use python program and library extensively to find the terminal velocity of rain drop. Graphs show close agreement and velocity power up to n=3 is good.***

Keywords— Rain drop, terminal velocity, air resistance, mass accretion.

1. INTRODUCTION

The major component of the water cycle is rain, responsible for depositing most of the fresh water on the earth and the major cause of rain production is moisture. Precipitation falls for enough moisture and upward motion of convective clouds (those with strong upward vertical motion such as cumulonimbus or thunder clouds) which can organize into narrow rain bands [1]. When upslope flow is maximized within windward sides of the terrain, heavy precipitation in mountainous areas is possible. On the leeward side of mountains, desert climates can exist due to the dry air caused by down slope flow which causes heating and drying of the air mass. Down slope flow causes heating and drying of the air mass on the leeward side of mountains and so desert climates can exist due to the dry air.

2. PHYSICAL PROPERTIES

Raindrops differ widely in their shapes, sizes and velocities. Smaller raindrops are generally spherical in shape. However, as size of the drop increases, it becomes an oblate spheroid. The raindrop is axially symmetric along the line of motion and in general non-spherical. The shape will be governed by internal hydrostatic pressure, hydrodynamic pressure of medium and surface tension. Beard and Chuang [2] describe the shape of a raindrop as a 10th order cosine distortion of a sphere as

$$r(\theta) = R(1 + \sum_{i=1}^{10} c_n \cos n\theta) \quad - (1)$$

Here R is the radius of the undistorted sphere in meter, c_n's are the coefficients that depend on the radius of the drop and θ is the polar angle of elevation.

Raindrops have a wide size distribution. A commonly used empirical distribution for rain drop size is the Marshall - Palmer distribution [3]

$$N(a) = 8 \times 10^6 e^{-8200 R h^{-0.21}} \quad - (2)$$

Here h is the rain rate given in mm/hr and $N(a)$ is the number of rain drops per unit volume that contains sizes within the interval $(R, R + dR)$. Large drops are severely distorted, while smaller drops are almost spherical. Note that the drops that make up a significant fraction of rain are less than 1mm in size and are not severely distorted and their shapes can be well approximated by a sphere. Therefore, in this paper, we will model rain drops as transparent spheres of water.

As a raindrop falls, it attains a constant velocity, called the terminal velocity [4]. Gunn and Kinzer [5] present an empirical study of the terminal velocities of falling raindrops for different drop sizes. Their observations show that the terminal velocity of a raindrop can be expressed as a function of its size and is given by

$$v_T = \sqrt{\frac{4g(2R)(\rho_w - \rho_a)}{b\rho_a}} \quad - (3)$$

Here v_T is in (meter/sec) and R is in meters. ~~Here~~ The first order differential equation of rain drop considering nth power of velocity for air resistance is solved for the first time by both analytically as well as using the library

of python code for no mass accretion which is based on the undergraduate theoretical knowledge. Emphasis is given so that undergraduate students can think of novel ideas; increase their skill of understanding; to create new method for proper understanding, etc.

3. THE PROBLEM

In general this kind of problem can be solved using time integral theorem which states that the time integral of force or impulse is equal to the integral of linear momentum. Mathematically we can write it as $\int \overrightarrow{dp} = \int \vec{F}\,dt$.

Let at time t the mass of a raindrop is m and velocity $\vec{v}$ and those at a later time $t + dt$ are $m + dm$ and $\vec{v} + \overrightarrow{dv}$ respectively. Thus $\vec{F}dt = (m + dm)(\vec{v} + \overrightarrow{dv}) - m\vec{v}$

Or, $$\vec{F} = m\frac{\overrightarrow{dv}}{dt} + \frac{dm}{dt}\vec{v} \qquad \text{- (4)}$$

In this case the motion will be governed by the weight of the raindrop $mg\hat{k}$, buoyant force $\frac{m\rho_a g}{\rho_w}\hat{k}$, and frictional force of the medium, which is proportional to the nth power of velocity $bv^n\hat{k}$ where ρ_a and ρ_w are the density of the medium and raindrop respectively. We assume $a = g(1 - \frac{\rho_a}{\rho_w})$ and then

$$m\frac{\overrightarrow{dv}}{dt} + \frac{dm}{dt}\vec{v} = am\hat{k} - bv^n\hat{k} \qquad \text{- (5)}$$

Here b is the resistive force per unit nth power of velocity. Lynch and Lommatsch [6] took the value of resistive constant as $b = 0.15\rho_a A$ where the cross sectional area of raindrop assumes the form $A = 3.3108 \times (2R)^{2.21672}$, with mass of raindrop as $m = 957.251 \times (2R)^{3.09275}$ where R is the approximate radius. Generally we put n=1 for resistive force proportional to velocity. But there are examples where n>1 and generalized procedure for solution is to be taken in those cases.

4. NO MASS VARIATION CASE

In this no mass variation case since $\frac{dm}{dt} = 0$ we get from equation (5) $$\frac{dv}{\frac{am}{b} - v^n} = \frac{bdt}{m} \qquad \text{- (6)}$$

When n=0 we have $v = a - \frac{bt}{m}$ and for $\frac{dv}{dt} = 0$ we have any value of the terminal velocity including zero because $am = b$ and thus clearly $am \geq b$.

For n=1 we have $v = \frac{am}{b}(1 - e^{-\frac{bt}{m}})$ and terminal velocity is $v_T = \frac{am}{b}$.

When n=2 the roots of $\frac{am}{b} - v^2$ are $\pm\sqrt{\frac{am}{b}}$ and the solution is $v = \sqrt{\frac{am}{b}}\frac{1-e^{-t\sqrt{\frac{4ab}{m}}}}{1+e^{-t\sqrt{\frac{4ab}{m}}}}$ $v = \sqrt{\frac{am}{b}}\frac{1-e^{-t\sqrt{\frac{4ab}{m}}}}{1+e^{-t\sqrt{\frac{4ab}{m}}}}$. Thus the terminal velocity can be obtained for $t \to \infty$ as $v_T = \sqrt{\frac{am}{b}}$.

When n=3 the roots of $\frac{am}{b} - v^3$ are $(\frac{am}{b})^{\frac{1}{3}}$, $\frac{-1\pm i\sqrt{3}}{2}(\frac{am}{b})^{\frac{1}{3}}$. Neglecting negative and imaginary terms as they have no physical meaning the solution is $v = (\frac{am}{b})^{\frac{1}{3}}[1 - e^{-(\frac{am}{b})^{\frac{2}{3}}\frac{3bt}{m}}]$. The terminal velocity can be obtained for $t \to \infty$ as $v_T = (\frac{am}{b})^{\frac{1}{3}}$.

When n=4 the roots of $\frac{am}{b} - v^4$ are $\pm(\frac{am}{b})^{\frac{1}{4}}$, $\pm i(\frac{am}{b})^{\frac{1}{4}}$. Hence $v = (\frac{am}{b})^{\frac{1}{4}}[1 - e^{-\frac{bt}{m}}]^{\frac{1}{4}}$. The terminal velocity for $t \to \infty$ as $v_T = (\frac{am}{b})^{\frac{1}{4}}$.

Using the procedure of rational fraction of integration the first order differential equation for nth power of velocity reduces to $$\int_0^v \sum_{l=1}^n \frac{s_l dv}{r_l - v} = \int_0^t \frac{bdt}{m} \Rightarrow e^{\frac{bt}{m}} = \prod_{l=1}^n (\frac{r_l}{r_l - v})^{s_l} \qquad \text{- (7)}$$

We can use another general procedure to solve equation (6). For that, we put $x = 1 - \frac{bv^n}{am}$ and take $p = \frac{n-1}{n}$. So $dx = -\frac{bnv^{n-1}dv}{am}$ and thus the equation reduces to $\frac{Amdx}{bnxv^{n-1}} = adt$

Or, $$-\frac{bndt}{m} = \frac{dx}{x[\frac{am}{b}(1-x)]^{\frac{n-1}{n}}} = \frac{dx}{x}\left[\frac{am}{b}(1-x)\right]^{-p} = \left(\frac{am}{b}\right)^{-p}\frac{dx}{x}\left[1 + px + \frac{p(p+1)}{2!}x^2 + \frac{p(p+1)(p+2)}{3!}x^3 + \cdots\right]$$

Or, $$-\left(\frac{am}{b}\right)^{p}\frac{bndt}{m}=\frac{dx}{x}\sum_{l=0}^{\infty}\frac{(p-1+l)!}{(p-1)!l!}x^{l}\Rightarrow-\left(\frac{am}{b}\right)^{p}\frac{bn(t+C)}{m}=\sum_{l=0}^{\infty}\frac{(p-1+l)!}{(p-1)!l!}\frac{x^{l}}{l}=\sum_{l=0}^{\infty}\frac{\left(l-\frac{1}{n}\right)!}{l\left(-\frac{1}{n}\right)!l!}\left(1-\frac{bv^{n}}{am}\right)^{l}$$

This is obtained by integration. Now at t=0 we have v=0 and $C=-\frac{m}{bn}\left(\frac{b}{am}\right)^{\frac{1-n}{n}}\sum_{l=0}^{\infty}\frac{\left(l-\frac{1}{n}\right)!}{l\left(-\frac{1}{n}\right)!l!}$. Thus

$$-\left(\frac{am}{b}\right)^{p}\frac{bnt}{m}=\sum_{l=0}^{\infty}\frac{\left(l-\frac{1}{n}\right)!}{l\left(-\frac{1}{n}\right)!l!}\left(1-\frac{bv^{n}}{am}\right)^{l} \qquad \text{- (8)}$$

5. DISCUSSIONS

Table 1

Air density ρ_a kg/m^3	0.006211*	Radius R m	0.0001– 0.01
Water density ρ_w kg/m^3	957.251*	$b=0.15\rho_a A$	4.91×10^{-12} – 6.84×10^{-5}
Acceleration due to gravity g m/s^2	9.81*	$a=g(1-\frac{\rho_a}{\rho_w})$	9.8099363

*ref [6]

For no mass accretion a python code is developed (matplotlib) and integration by odeint is (code is written in appendix) performed for different powers of velocity using the values of the parameters given in table 1. The plot in logarithmic scale is shown in figure 1 where velocity reaches its terminal velocity almost within ten seconds for mass of rain drop 0.5 mg and approximate diameter 1 mm. As discussed in section 4 the velocity for n=0 increases with time.

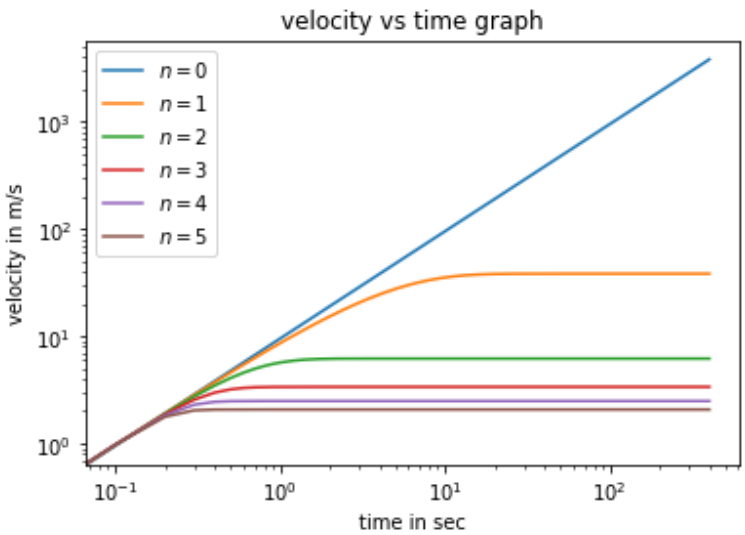

Figure 1

For further verification terminal velocity in logarithmic scale for n=1,2,3,4,5 is plotted against mass in logarithmic scale along with Gunn and Kinzer value [5]. This is shown in figure 2. The plots show close agreement and velocity power up to n=3 perhaps a better choice. Here n=0 is not plotted as the terminal velocity is undetermined.

The graphs contain a single intersecting point of approximate terminal velocity 1 m/s and mass 10^{-06} mg. This perhaps is the choice of minimum raindrop size below which it may be assumed to be a cloud particle. We note that terminal velocity satisfies the equation $bv_T^n = ma$ which depends on mass of raindrop and value of b. Here again best agreement between analytical and graphical value of v_T^n is observed.

6. CONCLUSIONS

These graphs clearly speak about the fact that diameter and mass have some impact on terminal velocity. Due to mass accretion in moist air the raindrop collects mass and rate may be $\frac{dm}{dt}=\rho_a vA$ where $A=\pi R^2$ is the projected area of the raindrop which is the largest cross section. For spherical drop, increase in radius is proportional to $m^{\frac{1}{3}}$ and an increase in area is proportional to $m^{\frac{2}{3}}$. Also mass accretion depends on velocity and so the raindrop size changes with time, i.e. dm/dt is proportional to mass m and velocity v. Thus $\frac{dm}{dt}=cm^{\alpha}v^{\beta}$ where c>0 is a constant and α and β are (almost) arbitrary

exponents [7-9]. This form includes the two most commonly studied cases called the easy case $(\alpha, \beta) = (\frac{2}{3}, 0)$ and the hard case $(\alpha, \beta) = (\frac{2}{3}, 1)$. The constant c depends on actual shape of raindrop. If the raindrop is spherical then [10]

$$c = \frac{\pi R^2}{(\frac{4}{3}\pi R^3 \rho_w)^\alpha} \quad - (9)$$

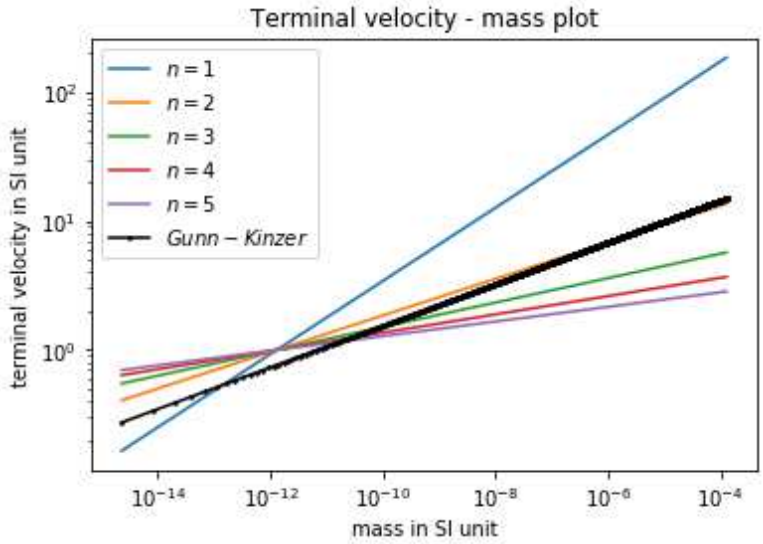

Figure 2

This modification seems inadequate because of pressure and temperature variations in the atmosphere. This is not considered in any literature so far.

7. ACKNOWLEDGEMENT

The first author did this whole work as online project fellow in covid situation under supervision of Dr. A. Ghorai at School of Science, Block 1/3G, 66/63 Jangalpur Road, Kolkata-81.

8. REFERENCES

[1] Kshitiz Garg and Shree K. Nayar, Photometric Model of a Rain Drop, www.semanticscholar.org @inproceedings 2003.
[2] K. V. Beard and C. Chaung. A new model for the equilibrium shape of raindrops. *Journal of Atmospheric Science*, vol. 44 no. (11), pp. 1509–1524, 1987.
[3] J. S. Marshall and W. M. K. Palmer. The distribution of raindrops with sizes. *Journal of Meteorology*, vol. 5, pp. 165–166, 1948.
[4] R. M. Manning. *Stochastic Electromagnetic Image Propagation*. McGraw-Hill, Inc, 1993.
[5] R. Gunn and G. D. Kinzer. The terminal velocity for water droplet in stagnant air. *Journal of Meteorology*, vol. 6, pp. 243–248, 1949.
[6] Ben Lynch and Gavin Lommatsch, Modeling the velocity of a raindrop, May 6, 2011, http://home2.fvcc.edu/~dhicketh/DiffEqns/Spring11projects/Ben_Lynch_Gavin_Lommatsch/DiffEqProject/DiffEqProjectGavinBen.pdf [8 August 2012]
[7] K. S. Krane, *American Journal of Physics* vol. 49, pp. 113–117, 1981; doi: 10.1119/1.12537.
[8] I. Adawi, *American Journal of Physics* vol. 54, pp. 739–740, 1986; doi: 10.1119/1.14465.
[9] Alan D. Sokal1, *American Journal of Physics* vol. 78, pp. 643-645, 2010; doi: 10.1119/1.3246871.
[10] M. H. Partovi and D. R. Aston, *American Journal of Physics* vol. 57, pp. 912–920, 1989; doi: 10.1119/1.15846.

9. APPENDIX

PYTHON CODE

Program for 1st graph :-

```
import numpy as np
from scipy.integrate import odeint
import matplotlib.pyplot as plt
d = 10**(-3) * 1
c = 0.3
pw = 1000
```

```
pa = 1.161 # at 300K, 1 bar
A = 3.3108*(d**2.21672)
m = 1000*0.957251*(d**3.09275)
g = 9.81
p =  g * (1-(pa/pw))
q = 0.5 * c * pa * A
v0=0
sol = [v0]
t= np.linspace(0,400,4000)
def f(v,t,n,a,b,ca):
   dvdt = (m*p - q*(v**n))/m - (ca*m**(a-1)*v**(b+1)) #raindrop motion equation
   return dvdt
for  n in range(0,6):
   sol = odeint(f,v0,t,args=(n,0,0,0))
   plt.plot (t,sol)
plt.title('velocity vs time graph with')
plt.yscale('log')
plt.xscale('log')
plt.legend(['$n=0$','$n=1$','$n=2$','$n=3$','$n=4$','$n=5$'])
plt.xlabel('time in sec')
plt.ylabel('velocity in m/s')
plt.show()
```

Program for 2nd graph For terminal velocity vs mass graph:-

```
from scipy.integrate import odeint
import numpy as np
import matplotlib.pyplot as plt
def f(v,t): return a - (b/m)*v**n
a=9.81*(1- 1.161/1000)
c = 0.3
pw = 1000
pa = 1.161 # at 300K, 1 bar
g = 9.81
for n in range(1,6):
   vt=[]
   M=[]
   Gn = []
   for d in np.arange(0.002*10**(-3),6*10**(-3),10**(-6)):
      b=(0.3*1.161*3.3108*d**2.21672)/2.0
      m=1000*0.957251*d**3.09275
      t=np.linspace(0,150,300)
      y0=0
      sol=odeint(f,y0,t)
      v=sol[:,0]
      vt.append(v[-1])
      M.append(m)
   plt.plot(M,vt)
for d in np.arange(0.002*10**(-3),6*10**(-3),10**(-6)):
   gn = (((4/3) * 9.81 * d * (pw-pa)) / (pa*c))**(0.5)
   Gn.append(gn)
plt.plot(M,Gn, color = 'black', marker = '.' , markerfacecolor = 'black', markersize = 3)
plt.subplot(111)
plt.xlabel('mass in SI unit')
plt.ylabel('terminal velocity in SI unit')
plt.yscale('log')
plt.xscale('log')
plt.title("Terminal velocity - mass plot")
plt.legend(['$n=1$','$n=2$','$n=3$','$n=4$','$n=5$','$Gunn-Kinzer$'])
plt.show()
```